Enhancing Single-Layer WSe2 Light Emission in Perylene-Doped Polymer Films through Efficient Energy Transfer

ADVANCED FUNCTIONAL MATERIALS
www.afm-journal.de

Enhancing Single-Layer WSe_2 Light Emission in Perylene-Doped Polymer Films through Efficient Energy Transfer

Marcos Gadea, Aswin Asaithambi, Raúl Bernabeu-Cabañero, Alex Farrando-Pérez, Maria Ramos, Juan C. Sancho-García, Ilka Kriegel, María A. Díaz-García, and M. Reyes Calvo**

The optical and mechanical properties of 2D semiconductors make them excellent candidates for the active components of plastic optoelectronic devices. Here, the integration of single-layer WSe_2 (1L-WSe_2) into a polystyrene (PS) film containing dispersed perylene orange (PDI-O) molecules is investigated. The findings reveal a notable enhancement in the light emission of 1L-WSe_2, which occurs exclusively upon PDI-O excitation and scales with the concentration of molecules in the PS film. Moreover, the increase in 1L-WSe_2 photoluminescence coincides with a quenching of the PDI-O light emission intensity and a decrease in its lifetime. These results point to efficient long-range interactions, such as Förster energy transfer, between PDI-O (acting as the donor) and 1L-WSe_2 (acting as the acceptor), as the mechanism responsible for the enhanced light emission in the latter. These findings are of great interest for the development of flexible optoelectronic devices integrating active 2D materials; the polymeric matrix plays a dual role, serving as both physical support and host for organic dopants that can optimize the light emission properties of the active 2D material.

1. Introduction

The discovery of 2D materials has sparked a revolution in materials science and nanotechnology, offering a plethora of applications in optoelectronics.[1,2] Among the wide variety of 2D materials, single-layer transition metal dichalcogenides (TMDs) have emerged as a particularly promising family of 2D semiconductors. The direct-bandgap electronic structure and large exciton binding energies in certain single-layer TMDs, such as MoS_2 or WSe_2, endow them with robust light-emission properties.[3,4] This positions single-layer TMDs as frontrunners for the development of next-generation optoelectronic devices, including photodetectors, solar cells, light-emitting diodes (LEDs),[5,6] and even lasers.[7,8]

In addition, 2D materials exhibit remarkable resilience to deformation, making them promising for integration into ultrathin flexible electronic and optoelectronic devices.[9–11] The integration of single layer semiconducting TMDs as active materials into hybrid structures with polymeric films has garnered considerable research interest, driven by the simplicity of preparation methods and the compatibility of 2D materials with solution-based processing techniques.[12] To date, 2D materials have been combined with polymeric substrates to implement

M. Gadea, A. Farrando-Pérez, M. Ramos[+], M. A. Díaz-García, M. R. Calvo
Departamento de Física Aplicada
Universidad de Alicante
Alicante E-03080, Spain
E-mail: maria.diaz@ua.es; reyes.calvo@ua.es

The ORCID identification number(s) for the author(s) of this article can be found under https://doi.org/10.1002/adfm.202401896

[+]Present address: CIC nanoGUNE Consolider, Donostia - San Sebastian E-20018, Spain

DOI: 10.1002/adfm.202401896

M. Gadea, A. Farrando-Pérez, M. Ramos[+], J. C. Sancho-García, M. A. Díaz-García, M. R. Calvo
Instituto Universitario de Materiales de Alicante (IUMA)
Alicante E-03080, Spain

A. Asaithambi, I. Kriegel
Functional Nanosystems
Istituto Italiano di Tecnologia
Genova 16163, Italy

R. Bernabeu-Cabañero, J. C. Sancho-García
Department of Physical Chemistry
University of Alicante
Alicante E-03080, Spain

M. R. Calvo
BCMaterials
Basque Center for Materials
Applications and Nanostructures
Leioa 48940, Spain

2D-material-based flexible field-effect transistors or light emitting devices.[9,10] They have also been covered by polymeric films for encapsulation purposes.[13,14] Notably, recent works propose embedding 2D materials in plastic optoelectronic architectures, where the polymeric matrix plays a functional role beyond merely serving as a substrate or capping layer. For instance, ongoing efforts to integrate 2D active materials with polymer-waveguides show promise for the development of photonic integrated circuits,[15–18] although examples of such integration remain scarce.

A challenging aspect for the application of 2D materials in plastic light-emitting devices is their modest quantum yields compared to typical molecular dyes used in plastic optoelectronics.[19] However, this limitation can be overcome by taking advantage of their outstanding tunability, allowing for the fine-tuning of their optical properties through various methods, such as functionalization or environmental control.[20,21] For instance, the photoluminescence (PL) of semiconducting TMD monolayers has been modulated by incorporating them into contact with other 2D materials in van der Waals heterostructures,[22–25] depositing them on different substrates or combining them with different active 0D systems.[26,27] Specifically, hybrid systems with various molecules, quantum dots or nanocrystals have been proposed to modify the PL emission of single-layer semiconducting TMDs.[28–32] Charge and energy transfer between 2D materials and 0D systems can play an important role in controlling the optical properties of 2D materials. For example, doping changes induced by charge transfer from different molecular systems directly deposited on top of single-layer TMDs has been shown to strongly enhance their PL intensity.[33,34] On the other hand, energy transfer processes have been demonstrated in a variety of 0D-2D material systems.[35–39] Specifically, long-distance Förster Energy transfer (FRET) between single-layer TMDs and different dyes,[35,37] quantum dots.[29,30,36,40] or nanocrystals.[31,32,41,42] has been reported. In most cases, the 2D material acts as an acceptor, with the 0D system serving as a donor. The resulting quench of the donor photoluminescence is often the main fingerprint of energy transfer and has been proposed for sensing applications.[43] Only scarcely has energy transfer from the 0D system been shown to increase the 2D material PL emission. Modest PL enhancement has been observed in single-layer $MoSe_2$ due to energy transfer from nanocrystals,[41] while a significant PL enhancement has been reported only in the case of WS_2 monolayers interacting with organic polymers.[38,44] or in close contact to quantum dot donors.[44]

On the other hand, perylenediimide (PDI) derivatives exhibit a unique blend of physical and chemical properties, showcasing thermal stability, high luminescence efficiency, redox capabilities, and high electron mobility.[45,46] These qualities make them promising candidates for applications in various fields such as photovoltaics and solar energy conversion.[47–49] The extended π-conjugation and rigid molecular structure of the PDI core leads to a high fluorescence quantum yield, making these derivatives attractive for purposes such as laser dyes,[50] fluorescent light collectors,[51] fluorescence sensors,[52] and emitters in organic light emitting diodes (OLEDs).[53] PDIs are known for being among the most photostable organic electronic materials in the literature, presenting promising opportunities for optoelectronic applications, particularly in the context of laser technologies.[54] For such purpose, the commercial derivative known as perylene orange (PDI-O) has demonstrated to be one of the best performing compounds of this family when dispersed in thermoplastic polymer matrices such as polystyrene (PS) and polymethylmethacrylate (PMMA).[54,55] However, the interaction of PDI molecules with 2D materials remains practically unexplored, with only a few recent reports on charge transfer between a PDI derivative and single-layer TMDs (i.e., 1L-MoS_2 or 1L-WSe_2).[56–58] when the PDI is covalently bound or directly deposited on the TMD.

Despite the extensive exploration of molecular dyes like PDI embedded in polymer films and the recent efforts to integrate 2D materials with polymer waveguides, the combination of both systems in polymeric structures – to potentially tune their properties based on their interplay – remains largely unexplored. To the best of our knowledge, the interaction between typical dyes used in plastic optoelectronics, such as PDIs, and common 2D semiconductors, such as single-layer TMDs, both embedded in polymer films, has not been previously investigated, despite holding significant promise for applications. In this work, we delve into the interplay between 1L-WSe_2 and PDI-O, both integrated into PS films. Through μ-PL and time resolved PL spectroscopy, we observed a remarkable enhancement of the 1L-WSe_2's PL, accompanied by a quenching of the PDI-O emission intensity and a decrease of its lifetime. We propose that these effects arise from the highly efficient energy transfer between the molecular donor (PDI-O) and the 2D acceptor (WSe_2 single layer). These results can therefore facilitate the integration and use of single-layer semiconductors in plastic photonic devices.

2. Results and Discussion

Our integrated system of study is illustrated in **Figure 1a**. The system consists of a single-layer flake of WSe_2 (1L-WSe_2) deposited onto a SiO_2/Si substrate, over which a thin polystyrene (PS) film, containing uniformly dispersed perylene orange (PDI-O) molecules has been spin-coated. PS has proved to be an excellent matrix to host photoluminescent organic compounds for waveguide-based lasers.[50,54,55,59] Similar results are expected for other polymeric matrices, such as PMMA, or others, whenever they have good transparency, enable a good dispersion of the organic compounds, and can be easily processed by spin-coating into low-loss waveguides.

The optical properties (absorption and PL) of the individual active components in the hybrid system (1L-WSe_2 and PDI-O) are shown in Figure 1b–d. During the sample preparation process, 1L-WSe_2 flakes are exfoliated onto transparent viscoelastic substrates (see Experimental Section). At this point, micro-reflectance spectroscopy measurements are performed (Figure 1b). The differential reflectance acquired on transparent substrates is directly related to the absorbance of 1L-WSe_2. Consequently, the resonances observed in the spectrum in Figure 1b correspond to absorption peaks associated with the formation of various excitonic states.[60] The excitonic peak with the lowest energy, denoted as X_A in Figure 1b, appears at ≈742 nm, corresponding to the so-called exciton A energy of ≈1.67 eV. The energy position of exciton peaks confirms the single-layer character of the flake.[60]

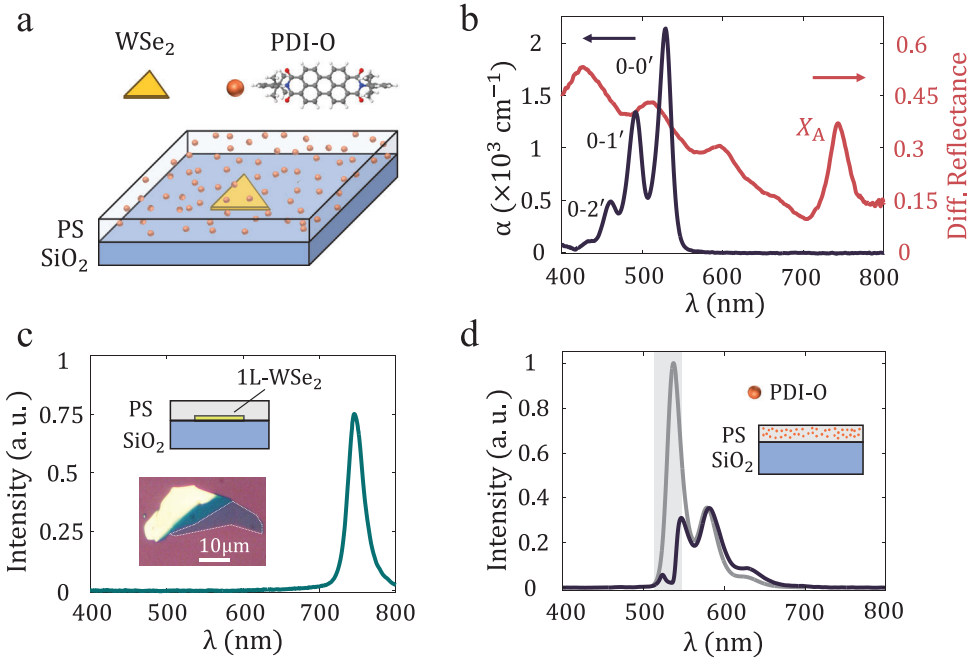

Figure 1. Sketch for the integrated system and optical properties of its individual components: WSe_2 single-layer flakes (1L-WSe_2) and perylene orange (PDI-O) molecules embedded in polystyrene (PS) films. a) Sketch illustrating a 1L-WSe_2 flake deposited onto a SiO_2/Si substrate, beneath a PS film with dispersed PDI-O molecules. b) Absorption coefficient (α) of a PS film doped with 1 wt% PDI-O (purple line, left axis), and differential reflectance spectrum of a 1L-WSe_2 deposited on PDMS (red line, right axis). c) μ-PL spectrum measured at a 1L-WSe_2 nanoflake deposited on SiO_2/Si substrate after being covered with a 100 nm PS film. Excitation wavelength is 532 nm. Inset: Optical microscopy image in reflection mode of the flake. d) μ-PL of PDI-O molecules dispersed in a PS film deposited on a SiO_2/Si substrate using the same confocal setup (see Experimental Section) as for 1L-WSe_2 (solid line) and macroscopic measurement of PDI-O's PL in a fluorometer (dashed line). The grey area indicates the wavelength range of the notch filter used in the confocal setup.

Additionally, in Figure 1b, we also present the absorption spectrum of a PDI-O-doped (1 wt%) PS thin film spin-coated over fused silica. This spectrum was acquired using a standard spectrophotometer (see Experimental Section for more details) in the absence of any 2D material. The absorption spectrum reveals the vibrational structure of the molecule,[54,55] with a primary transition (0-0′) observed at 530 nm and the vibrational peaks (0-1′) at 490 nm and (0-2′) at 460 nm.

Selected 1L-WSe_2 flakes were transferred onto SiO_2/Si substrates, and PS films (without any dopants) were subsequently spin-coated on top of them. The embedded flakes were characterized by micro-photoluminescence (μ-PL) spectroscopy in a confocal configuration, as described in the Experimental Section. Figure 1c presents the μ-PL spectrum of a 1L-WSe_2 flake after the deposition of a 100 nm PS film (λ_{exc} = 532 nm). The spectrum exhibits a strong emission peak centred at λ_{WSe_2} = 747 nm (1.66 eV), associated with the radiative recombination of the A exciton.[61] The results indicate that at least 70% of the μ-PL intensity remained after PS deposition (see Figure S1, Supporting Information). This reduction in intensity can be attributed to the partial absorption of the PL signal by the PS film, to changes in the electronic properties of the 1L-WSe_2 due to the presence of PS, or due to scattering by the polymer covering the 1L-WSe_2 flake.

On the other hand, PS films incorporating PDI-O molecules (PS/PDI-O) were spin-coated on SiO_2/Si substrates and characterized with the same confocal μ-PL setup employed for the study of the 2D material (see inset of Figure 1d). The μ-PL spectrum obtained for a PS/PDI-O (1 wt%) film using λ_{exc} = 532 nm (solid line in Figure 1d) closely resembles the one obtained from characterizing a similar film on a transparent substrate using a fluorometer (gray line in Figure 1d) (see Experimental Section). Note that the lower intensity of the 0-0′ PL peak in the μ-PL confocal measurement results from the use of a notch filter, necessary for removing the back-scattered light from the excitation line. Despite this, confocal μ-PL measurements still capture a significant portion of the total PL spectrum of the PDI-O molecule, with a maximum around $\lambda_{PDI\text{-}O}$ = 550 nm.

The light emission properties of the integrated samples (see inset of **Figure 2a**), where the 2D material (1L-WSe_2) is embedded in PS films containing dispersed PDI-O molecules (PS/PDI-O), are presented in Figure 2. Specifically, in Figure 2a, μ-PL spectra are displayed for 1L-WSe_2 flakes beneath 100 nm PS films containing different PDI-O concentrations (0.5-2 wt%). The excitation wavelength was set to λ_{exc} = 532 nm, absorbed by both PDI-O and 1L-WSe_2. It should be noted that given the significantly higher quantum yield of PDI-O compared to that of 1L-WSe_2, the PL signal from PDI-O was filtered out to maximize the detection of the 1L-WSe_2 emission (see Experimental Section). Additionally, to capture the overall behaviour of the samples, each μ-PL spectrum in Figure 2a is the outcome of averaging several spectra taken at different locations within the same 1L-WSe_2 flake. In fact, we acquired μ-PL maps (see example in Figure 2b,c) that served to confirm that the PL signal

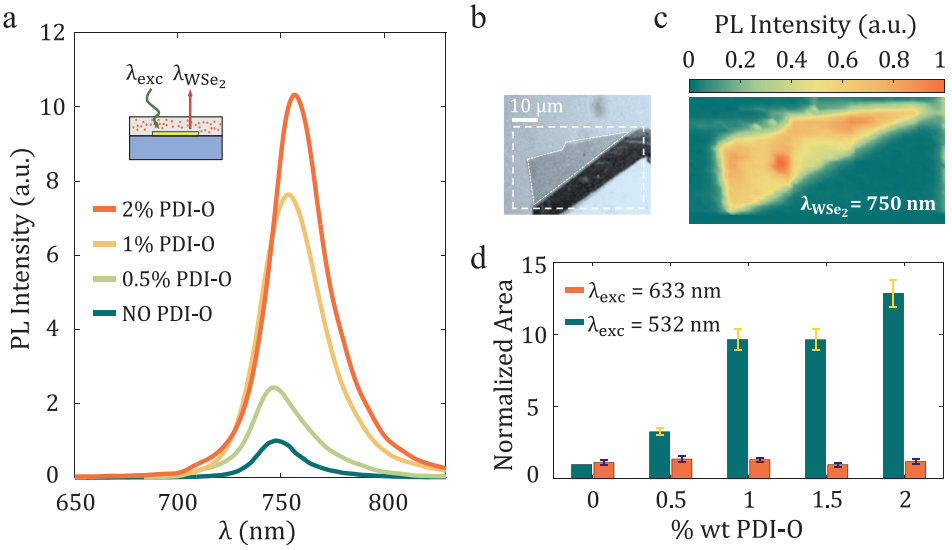

Figure 2. μ-PL spectroscopy for 1L-WSe_2 flakes integrated with PS films containing dispersed PDI-O (PS/PDI-O). a) μ-PL spectroscopy for 1L-WSe_2 flakes (λ_{exc} = 532 nm) covered with a 100 nm thick PS film containing different concentrations of PDI-O molecules (0, 0.5, 1, and 2 wt%) as indicated in the legend. Inset: Sketch for 1L-WSe_2 on a SiO_2/Si substrate, beneath a 100 nm thick PS/PDI-O film. b) Optical microscopy image in reflection mode of a 1L-WSe_2 flake beneath a 1 wt% PS/PDI-O film (the single-layer area is marked with a white continuous line) c) μ-PL intensity map at λ_{WSe_2} = 750 nm, (λ_{exc} = 532 nm) for the 1L-WSe_2 flake shown in panel (b). The map was acquired at the area enclosed by the dashed line in (b). d) Integrated PL intensity for spectra acquired on samples with varying PDI-O concentrations, using two different excitation wavelengths, 532 and 633 nm, respectively. Data is normalized to the intensity of the 1L-WSe_2 flake under PS with no PDI-O.

remains constant, with small fluctuations, across the entire flake area.

A remarkable result according to Figure 2a is the significant increase in the PL emission of 1L-WSe_2 upon the introduction of the PDI-O molecules in the PS films, compared to samples without PDI-O. This rise in 1L-WSe_2 PL intensity with the increasing PDI-O concentration suggests the interaction between the active components as the key factor behind this enhancement. A precise quantification of the 1L-WSe_2 PL enhancement as a function of the PDI-O concentration is presented in Figure 2d, where the integrated intensity for the PL spectra from Figure 2a is compared. Notably, the PL emission of 1L-WSe_2 increases more than 10 times for 2 wt% PDI-O compared to samples covered by polystyrene with no PDI-O and ≈8 times when compared to pristine flakes (see Table S1, Supporting Information). While the 1L-WSe_2 PL increases with PDI-O concentration following an approximately linear trend up to 1 wt%, for higher values (i.e., 2 wt%), the PL rise seems to saturate. This is attributed to the formation of molecular aggregates when PDI-O is dispersed in PS around this concentration, as documented in previous studies related to the use of these materials as active compounds of organic lasers.[59] Quantum-chemical calculations (see notes in the section S3 of the Supporting Information) allowed us to confirm the evolution of the PDI-O optical properties upon molecular aggregation. Actually, from a selected set of different dimeric configurations explored, structurally and energetically viable, one can observe a marked reduction of the transition dipole moment going from an isolated molecule to an aggregated system (see notes included in the section S3, Supporting Information). The formation of these aggregates adversely impacts the emission efficiency of PDI-O,[62] thereby likely accounting for the observed trend in Figure 2d.

To further confirm that the enhancement of the 1L-WSe_2 PL emission stems from the interaction with the PDI-O molecules, we carried out μ-PL experiments for the same samples under excitation at λ_{exc} = 633 nm, a wavelength that cannot be absorbed by PDI-O. In contrast to the λ_{exc} = 532 nm data, no significant differences in the PL intensity of the 1L-WSe_2 flakes were observed at λ_{exc} = 633 nm with varying PDI-O concentration (see Figure S7, Supporting Information). The corresponding 1L-WSe_2 integrated PL intensity values for different PDI-O concentrations have been included in Figure 2d for comparison. Hence, we establish that the PL enhancement in the 1L-WSe_2 flakes occurs exclusively when the PDI-O molecule is also photoexcited. This confirms that the enhancement of the 1L-WSe_2's PL arises from its interaction with the photo-excited PDI-O, allowing us to dismiss alternative origins, such as the constructive interference in the multilayer system formed by the substrate's SiO_2 layer and the PS thin film. Moreover, similar results were obtained for samples prepared on quartz substrates (see Figure S8, Supporting Information), further discarding any possible influence from the substrate.

To gain insights into the interaction mechanisms between the 2D material and the PDI-O, we analyzed the μ-PL emission of the PDI-O molecules in the integrated system (see **Figure 3**), concentrating on the spectral region where PDI-O emits (between 530 and 630 nm). Figure 3a presents a comparison between PDI-O PL spectra taken at locations on and off the 1L-WSe_2 flake area (illustrated in the inset of Figure 3a with a blue (on) and purple (off) arrow, respectively) for a sample with 100 nm thick PS film containing 1 wt% PDI-O. A significant decrease in the PDI-O PL signal of ≈30% can be observed when the molecules lie above the 1L-WSe_2. A similar quenching rate is observed for samples with other PDI-O concentrations (see Figure S9, Supporting

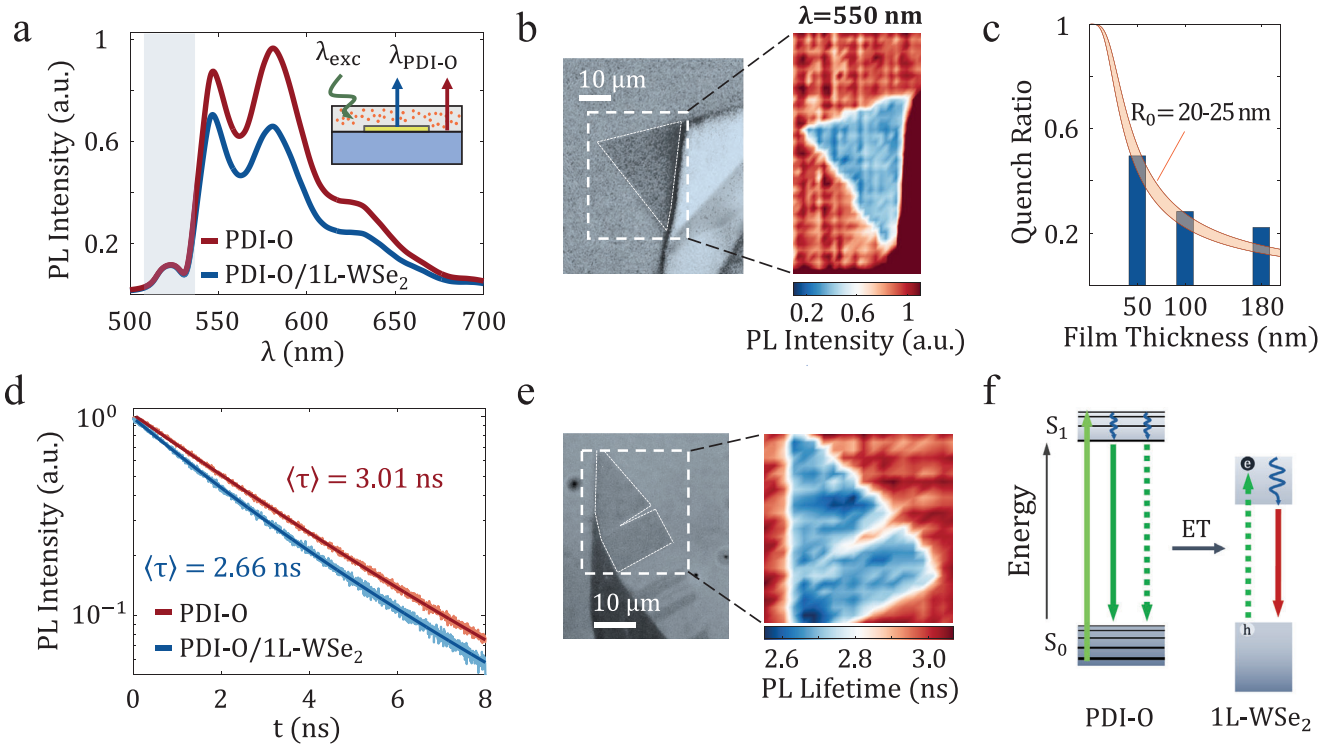

Figure 3. μ-PL spectroscopy for the PDI-O molecules dispersed in PS in the integrated samples with 1L-WSe_2. a) μ-PL intensity collected in two different regions of a 100nm thick PS/PDI-O sample, in locations on and off the 1L-WSe_2 flake respectively. b) Left: optical microscopy image in reflection mode of a 1L-WSe_2 sample beneath a 100 nm PS/PDI-O film. Right: μ-PL map at λ = 550 nm for the same sample. c) Quench ratio of the PDI-O μ-PL, calculated from the intensity measured on top of the 1L-WSe_2 in relation to the signal measured at regions off the flake for varying thicknesses of the PS/PDI-O film (blue bars). The orange shadowed area represents the estimated quench ratio for a Förster radius of 20–25 nm. d) Time-resolved PL measurements for PS/PDI-O on and off the 1L-WSe_2 flake area. e) Left: optical microscopy image in reflection mode of a 1L-WSe_2 flake (marked with a white, continuous line) beneath a 50 nm thick PS/PDI-O film. Right: averaged PL lifetime map obtained from the time-resolved PL measurements conducted in the outlined region of the image on the left. f). Illustration of the optical transitions and energy transfer process for PDI-O (donor) and 1L-WSe_2 (acceptor). Straight vertical arrows denote light absorption (upward) and emission (downward), whereas vibrational relaxation is depicted through undulating arrows. Dashed-line arrows represent the optical transitions involved in the energy transfer process.

Information). Each spectrum in Figure 3a corresponds to the average of several spectra taken at different positions on and off the flake, respectively. In fact, we acquired μ-PL maps at lambda = 550 nm, such as the one presented in Figure 3b, that clearly show a significant and uniform decrease of the emission intensity from PDI-O for all locations above the 1L-WSe_2 flake. Note that we performed the μ-PL measurements in a confocal configuration using a notch filter centered at λ = 532 nm, missing part of the PDI-O spectrum.

The observed quenching in PDI-O's PL intensity, together with the enhancement in 1L-WSe_2's emission, suggests an interplay between the two active components which could be mediated by either charge or energy transfer from PDI-O to 1L-WSe_2. Charge transfer effects require large orbital overlap, scaling with distance as r^{-12}, and imply close contact between the molecules and the 2D material. In our system, we anticipate that the number of PDI-O molecules at a short enough distance from 1L-WSe_2 for charge transfer is negligible, compared to the majority of dispersed molecules, which are located at greater distances and for which PS acts as a spacer. Similarly, Dexter energy transfer has a comparable distance scaling as charge transfer processes, requiring also significant orbital overlap. Therefore, these processes might only account for a marginal fraction of the observed quenching (see notes in section S7 (Supporting Information) for an estimation. Furthermore, a recent work in Ref. [56] reported charge transfer from PDI-O molecules directly evaporated on top of 1L-WSe_2. Völzer et al.[56] propose a type II alignment for the PDI-O/1L-WSe_2 system, which results in the quenching of both PDI-O and 1L-WSe_2 PL. Hence, while we cannot discard the occurrence of charge transfer from the closest molecules to the 2D material, the magnitude of the PDI-O PL quenching in our results, along with the significant enhancement of the 1L-WSe_2 PL, cannot be justified by charge transfer or other short-distance interaction mechanisms. On the contrary, our findings point to long distance interactions, such as Förster resonance energy transfer (FRET). FRET, involving dipole-dipole interactions, has indeed been reported for various combinations of 2D and 0D materials.[35,36]

To validate a FRET interpretation of our results, we investigated the dependence of the system interactions on the distance between the molecules and the 1L-WSe_2 flake. For this purpose, we prepared samples with PS films of varying thicknesses (50-200 nm), while maintaining a fixed PDI-O concentration at 1 wt%. To quantify the quenching of the PDI-O's μ-PL signal, we define a quench ratio (QR) as $QR = 1 - I_{PDI-O/WSe_2}/I_{PDI-O}$. I_{PDI-O} represents the integrated μ-PL intensity for PS/PDI-O

acquired at locations outside of the 1L-WSe_2 area, i.e., PDI-O not interacting with the 2D material. Correspondingly, I_{PDI-O/WSe_2} represents the integrated μ-PL intensity for PS/PDI-O on the 1L-WSe_2 flake. In Figure 3c, the value of QR is presented as a function of the PS/PDI-O film thickness, revealing a greater quenching of the PDI-O emission with the reduction in film thickness. This result can be qualitatively explained as follows: for a given characteristic interaction length, the proportion of dye molecules situated close enough to interact with the 1L-WSe_2 relative to the total is larger for thinner films. While the QR for PDI-O is strongly affected, the 1L-WSe_2 PL enhancement barely changes with film thickness (Figures S10 and S11, Supporting Information).

In a FRET scenario, the scaling with distance of the energy transfer efficiency (ϕ) strongly depends on the dimensionality of the system. The typical FRET scaling as r^{-6} for 0D-0D systems (e.g., molecule–molecule interactions) transforms into r^{-4} for 0D donors (molecules, q-dots, etc.) and 2D acceptors (see Ref. [63] for example), substantially increasing the interaction range. Therefore, for our system, the FRET efficiency between PDI-O (0D donor) and 1L-WSe_2 (2D acceptor) would be given by:[31,64]

$$\phi(r) = \frac{1}{1+\left(\frac{r}{R_0}\right)^4} \tag{1}$$

where the interaction length-scale is defined by the Förster radius (R_0), distance at which 50% of the excitation energy is transferred from the donor to the acceptor, and r is the distance from a given PDI-O molecule to the 1L-WSe_2 flake. The emission intensity (I_{PDI-O}) of a PDI-O molecule located at a distance r of the flake would be given by:[31,65]

$$I_{PDI-O}(r) = I^0_{PDI-O}\ (1-\phi(r)) \tag{2}$$

where I^0_{PDI-O} is the emission intensity of PDI-O donor in absence of energy transfer. According to Equation (2), the PL intensity of a molecule located at a distance R_0 from the flake is quenched to a half. By summing up the contributions to the μ-PL signal from molecules at different distance r within the PS film –each showing different degrees of quenching– we can estimate the QR for the PDI-O μ-PL signal in our samples (see Figure S12 Supporting Information). The comparison of this estimation to the experimental data (see Figure 3c; Figure S12, Supporting Information) suggests a Förster radius value of R_0 ≈20–25 nm for our system.

FRET typically results not only in the quenching of the donor's PL intensity, but also in a reduction in its emission lifetime. This prompted us to perform time-resolved spectroscopy experiments (Figure 3d,e). In Figure 3d, the PS/PDI-O PL time decay for a 50 nm PS film (1 wt% PDI-O) is presented at locations on and off the 1L-WSe_2 flake. The PL decay is faster for PDI-O on top of 1L-WSe_2 compared to positions outside the flake, in line with a FRET interpretation. Time-resolved spectroscopy of PDI-O is typically modelled by a double exponential function, accounting for the different lifetimes of the optical transitions contributing to the PL emission and the presence of molecular interactions or aggregation effects.[59,62] Fitting to a bi-exponential function (see Table S2, Supporting Information) yields averaged lifetimes $\langle\tau_{PDI-O}\rangle$ = 2.66 ns and $\langle\tau^0_{PDI-O}\rangle$ = 3.01ns for spectra acquired on and off the 1L-WSe_2, respectively (Figure 3d). The averaged lifetimes manifest a qualitative decrease of the PDI-O lifetime due to the interaction with the 2D material. The analysis of time decays acquired at different positions over the samples produces lifetime maps, such as the one displayed in Figure 3e. The map confirms a consistent decrease in the PDI-O´s PL lifetime across the entire area of the 1L-WSe_2 flake compared to the outside region (see Figure 3e).

Because of FRET, the lifetime of a given PDI-O donor (τ_{PDI-O}) depends on the distance r between the molecule and the 2D material:[31]

$$\tau_{PDI-O}(r) = \tau^0_{PDI-O}\ (1-\phi(r)) \tag{3}$$

where τ^0_{PDI-O} is the donor lifetime in absence of energy transfer. According to expressions 2 and 3, PDI-O molecules would display varying degrees of intensity and lifetime quenching of their emission based on their distance r to the 1L-WSe_2. To model our measurements, which comprise the emission from molecules distributed within the PS film, we add the contributions from molecules located at all possible distances within the film. From a comparison with the experimental results, we estimate that our lifetime measurements in Figure 3d are compatible with a Förster radius value $R_0 \approx 20$ nm (see Figures S13-15, Supporting Information). Similar time-decay studies for samples with thicker PS/PDI-O films yield smaller changes in the PDI-O lifetime in presence of 1L-WSe_2 (Table S2, Supporting Information)., these findings align with the proposed interpretation (see Figure S14, Supporting Information).

The extracted value $R_0 \approx$ 20–25 nm falls among the largest reported interaction lengths for energy transfer between 0D donors and 2D acceptors, such as ≈ 20 nm for graphene and rhodamine.[63] and ≈30 nm in the case 1L-MoS_2 and quantum well nanoplatelets.[42] The Förster radius, R_0, depends on different parameters: i) the spectral overlap between acceptor's absorption and donor's emission, large in our system (see Figure S17, Supporting Information); ii) the donor's quantum yield, reported for PDI-O molecules in solid films with high values up to 0.85;[66] and iii) the environmental dielectric screening. In this regard, the lower permittivity of PS (ϵ_r = 2.46).[67] in comparison to other spacers such as h-BN allows for a longer range of dipole-dipole interactions. The comparison to other 0D-2D systems suggests that energy transfer is highly efficient in the PS/PDI-O/1L-WSe_2 system, resulting in a strong quenching of PS/PDI-O´s PL. Likely, this also underlies the observed enhancement of the 1L-WSe_2 emission. Up to date, a large FRET-induced enhancement of the 2D material's PL has been rarely observed and, to our knowledge, only for 1L-WS_2 in intimate contact with quantum dots.[44]

Following consideration from a FRET model, the 1L-WSe_2's PL enhancement $\frac{I_{WSe_2}(r)}{I^0_{WSe_2}}$ due to a PS/PDI-O thin slab located at a distance r from the 2D material flake is approximately given by:[31]

$$\frac{I_{WSe_2}(r)}{I^0_{WSe_2}} = 1 + \frac{\alpha_{PS/PDI-O}(\lambda_{exc})\ T_{PS/PDI-O}}{\alpha_{1L-WSe_2}(\lambda_{exc})\ T_{1L-WSe_2}}\ \phi_{ET}(r) \tag{4}$$

which depends on the absorbance of the two active components, given by their absorption coefficients (α) at the excitation

wavelength (λ_{exc} = 532 nm) and their respective thicknesses (T). By adding contributions from the whole film (see Figure S16, Supporting Information) and assuming $R_0 \approx 20$ nm, we estimate a PL enhancement of ≈1.5 times for 1L-WSe_2 embedded within a 1 wt% PS/PDI-O film. This value is considerably smaller than our experimental observation (≈10 times). The expected enhancement barely depends on films thickness (see Figure S16, Supporting Information). Therefore, this discrepancy can be only explained by limitations of the considered model or by the following considerations regarding 1L-WSe_2´s absorption coefficient. The enhancement of the acceptor's emission strongly depends on the relative absorbance of both acceptor and donor at the excitation wavelength (see Equation (4)). In our estimation, we used the measured absorption coefficient values of PS/PDI-O films (Figure 1b). However, for 1L-WSe_2, we assumed the absorption coefficient values for pristine samples on SiO_2/Si from Ref. [68] The presence of the PS film may significantly alter the dielectric screening and doping of 1L-WSe_2, impacting the electronic and excitonic properties of the material. This impact is evident in the observed ≈30% reduction of the 1L-WSe_2 PL intensity when integrated into PS compared to the pristine samples (Figure S1, Supporting Information). We believe that the influence of PS could substantially modify the absorption properties of 1L-WSe_2, explaining the discrepancy between the expected and measured enhancement values. In fact, Ref. [30] shows how even moderate changes in the absorption of 1L-TMDs can lead to significant modifications in the energy transfer efficiency from 0D systems.

3. Conclusion

We observed a remarkable tenfold enhancement in the photoluminescence of 1L-WSe_2 when embedded in PS thin films containing dispersed PDI-O molecules. This enhancement appears accompanied by a quenching of the PDI-O light emission, both in intensity and lifetime. These findings point to the presence of underlying long-range interaction mechanisms, such as FRET, from PDI-O (donor) to 1L-WSe_2 (acceptor), with the PS matrix serving as a spacer. This interpretation is supported by the large spectral overlap between the two active systems. Furthermore, the significant PDI-O´s emission quenching and its increase with reducing the PS film thickness suggest an unusually large interaction length compared to other systems involving molecular donors and single-layer acceptors. This implies a highly efficient energy transfer, likely responsible for the substantial increase in 1L-WSe_2 emission. Our results hold promise for the development of flexible plastic optoelectronics devices incorporating active 2D materials, where the polymeric matrix can provide physical support and serve as a functional element, such as a waveguide. Beyond mere structural roles, the polymer film can host molecular dopants, enabling the fine-tuning of the properties of 2D materials through tailored interactions. In particular, our results demonstrate that this approach has the potential to enhance the light emission of 2D semiconductors, with the capacity to overcome their limitations toward their application as active materials in plastic light-emitting devices. There is ample opportunity for further improvement in emission by exploring alternative combinations of 2D and molecular compounds. Furthermore, energy transfer with molecular systems could enable flexible devices with improved efficiency, leveraging the unique properties of 2D materials, such as flexible photodetectors, excitonic light emitters, or strain sensors.

4. Experimental Section

Materials: Chemicals were purchased from commercial sources and used without further purification. PS (M = 35 000 g mol^{-1}) and toluene (≥ 99.7%) were purchased from Sigma-Aldrich. PDI-O (M = 711 g mol^{-1}) was purchased from Phiton with a purity higher than 99.5%. WSe_2 bulk crystals were purchased from HQ Graphene.

Sample Preparation: The PS thin films were prepared by the spin-coating technique. Solutions containing PS and a varying amount of PDI-O were prepared and cast over SiO_2/Si substrates. The amount of PS relative to the amount solvent (toluene) was adjusted to obtain the desired film thickness.[50,55] Film thickness was confirmed by transmittance and reflectance measurements.[67]

For 1L-WSe_2, bulk crystals were mechanically exfoliated onto transparent Gel film substrates (Gel-Pak, WF x4 6.0mil). The determination of the WSe_2 flake thickness was carried out using optical microscopy and micro-reflectance spectroscopy.[60] Once the single-layer flakes were identified, they were deliberately placed onto 300 nm SiO_2/Si substrates though the deterministic dry transfer method.[69] The SiO_2/Si substrates provided a good color contrast for single-layer flakes, which can be difficult to trace once beneath the PS films when on transparent substrates.

Optical Characterization: Absorption and PL spectroscopies on PS/PDI-O films were conducted using a Jasco V-650 spectrophotometer and a Jasco FP-6500/6600 fluorimeter, respectively. The PL measurements employed an excitation wavelength of 490 nm.

μ-PL spectroscopy performed in a home-made confocal setup employing an excitation and collection spots of ≈1 μm and ≈8 μm diameter, respectively. A solid-state laser with an emission wavelength of 532 nm was used for excitation at a power of ≈80 μW measured at the sample location. To obtain the PL of PDI-O, a notch filter centred at $\lambda = 533 \pm 2$ nm (full width at half maximum, FWHM = 17 nm) was employed to remove the signal coming from excitation line. To optimize the detection of the 1L-WSe_2 PL, a 700 nm long pass filter was employed to limit the contributions from the PDI-O PL as well as from the reflected laser excitation. To reduce fluctuations, μ-PL maps are recorded, for which spectra are taken at several different spatial locations from each sample. Depending on the size area of the 1L-WSe_2 flakes, for each sample, data from at least twelve and up to a hundred of points are averaged. For μ-PL measurements performed on PS/PDI-O regions off the flakes, hundreds of points are typically averaged. The integrated intensity is obtained as the mean values from those measurements and error is estimated as their standard deviation.

Time resolved μ-PL spectroscopy: A pulsed laser PiL040-FS with an emission wavelength centered at 405 nm, 10 MHz repetition rate with < 45 ps pulse width from NKT photonics was used for excitation at a power of 1 μW. The excitation laser was coupled into IX83 Olympus microscope and focused on the sample with a 50X microscope objective lens (NA = 0.8). The PL emission was then collected and collimated using the same objective lens used for detection and an avalanche photo-diode couple to PicoHarp 300 (PicoQuant) time correlated single photon counting (TC-SPC) system.

Supporting Information

Supporting Information is available from the Wiley Online Library or from the author.

Acknowledgements

The authors acknowledge funding from the Spanish MCIN through grants PID2020-119124RB-I00, PID2019-106114GB-I00, CNS2023-145151 (funded by MCIN/AEI/10.13039/501100011033 and from European

Union "NextGenerationEU"/PRTR), MFA/2022/045 (funded by Generalitat Valenciana and from European Union NextGenerationEU). This work has also been funded by the Generalitat Valenciana through grants IDIFEDER/2020/005, IDIFEDER/2021/016, the APOSTD/2020/249 fellowship for M.R., support from the Plan Gen-T of Excellence for M.R.C (CideGenT2018004), and the Prometeo 2021/017 project. A.A. and I.K acknowledge the support of European Union's Horizon 2020 European Research Council, under grant agreement no. 850875 (I.K.) (Light-DYNAMO) and I.K. acknowledge European Union's Horizon 2020 Research and Innovation program under grant agreement no. 101017821 (I.K.) (LIGHT-CAP).

Conflict of Interest

The authors declare no conflict of interest.

Data Availability Statement

The data that support the findings of this study are available from the corresponding author upon reasonable request.

Keywords

2D-materials, energy transfer, perylene orange, photoluminescence, plastic optoelectronics

Received: January 31, 2024
Revised: May 3, 2024
Published online: May 27, 2024

[1] K. F. Mak, J. Shan, *Nature Photon.* **2016**, *10*, 216.
[2] W. Zhang, Q. Wang, Y. Chen, Z. Wang, A. T. S. Wee, *2D Mater.* **2016**, *3*, 022001.
[3] K. F. Mak, C. Lee, J. Hone, J. Shan, T. F. Heinz, *Phys. Rev. Lett.* **2010**, *105*, 136805.
[4] A. Splendiani, L. Sun, Y. Zhang, T. Li, J. Kim, C. Y. Chim, G. Galli, F. Wang, *Nano Lett.* **2010**, *10*, 1271.
[5] J. S. Ross, P. Klement, A. M. Jones, N. J. Ghimire, J. Yan, D. G. Mandrus, T. Taniguchi, K. Watanabe, K. Kitamura, W. Yao, D. H. Cobden, X. Xu, *Nature Nanotech.* **2014**, *9*, 268.
[6] F. Withers, O. Del Pozo-Zamudio, A. Mishchenko, A. P. Rooney, A. Gholinia, K. Watanabe, T. Taniguchi, S. J. Haigh, A. K. Geim, A. I. Tartakovskii, K. S. Novoselov, *Nature Mater.* **2015**, *14*, 301.
[7] S. Wu, S. Buckley, J. R. Schaibley, L. Feng, J. Yan, D. G. Mandrus, F. Hatami, W. Yao, J. Vuckovic, A. Majumdar, X. Xu, *Nature.* **2015**, *520*, 69.
[8] Y. Ye, Z. J. Wong, X. Lu, X. Ni, H. Zhu, X. Chen, Y. Wang, X. Zhang, *Nature Photon.* **2015**, *9*, 733.
[9] L. Gao, *Small.* **2017**, *13*, 1603994.
[10] D. Akinwande, N. Petrone, J. Hone, *Nat. Commun.* **2014**, *5*, 5678.
[11] T. Mueller, E. Malic, *npj 2D Mater Appl.* **2018**, *2*, 29.
[12] J. Kim, O. Song, Y. Cho, M. Jung, D. Rhee, J. Kang, *ACS Mater. Au.* **2022**, *2*, 382.
[13] P. J. Jeon, S. W. Min, J. S. Kim, S. R. A. Raza, K. Choi, H. S. Lee, Y. T. Lee, D. K. Hwang, H. J. Choi, S. Im, *J. Mater. Chem. C.* **2015**, *3*, 2751.
[14] F. Carrascoso, H. Li, J. M. Obrero-Perez, F. J. Aparicio, A. Borras, J. O. Island, A. Barranco, A. Castellanos-Gomez, *npj 2D Mater Appl.* **2023**, *7*, 24.
[15] Y. Tan, R. He, C. Cheng, D. Wang, Y. Chen, F. Chen, *Sci. Rep.* **2014**, *4*, 7523.
[16] J. H. Kim, J. Lee, C. Seo, G. H. Han, B. W. Cho, J. Kim, Y. H. Lee, H. S. Lee, *Nano Lett.* **2023**, *23*, 11019.
[17] A. Frank, J. Zhou, J. A. Grieve, I. Verzhbitskiy, J. Viana-Gomes, L. Loh, M. Schmid, K. Watanabe, T. Taniguchi, G. Eda, A. Ling, *Adv. Opt. Mater.* **2022**, *10*, 2101684.
[18] F. Auksztol, D. Vella, I. Verzhbitskiy, K. F. Ng, Y. W. Ho, J. A. Grieve, J. Viana-Gomes, G. Eda, A. Ling, *ACS Photonics.* **2019**, *6*, 595.
[19] S. Roy, A. S. Sharbirin, Y. Lee, W. B. Kim, T. S. Kim, K. Cho, K. Kang, H. S. Jung, J. Kim, *Nanomaterials.* **2020**, *10*, 1032.
[20] J. Ji, J. H. Choi, *Nanoscale.* **2022**, *14*, 10648.
[21] S. Bertolazzi, M. Gobbi, Y. Zhao, C. Backes, P. Samorì, *Chem. Soc. Rev.* **2018**, *47*, 6845.
[22] L. Wu, Y. Chen, H. Zhou, H. Zhu, *ACS Nano.* **2019**, *13*, 2341.
[23] G. Froehlicher, E. Lorchat, S. Berciaud, *Phys. Rev. X.* **2018**, *8*, 011007.
[24] X. Liu, J. Pei, Z. Hu, W. Zhao, S. Liu, M. R. Amara, K. Watanabe, T. Taniguchi, H. Zhang, Q. Xiong, *Nano Lett.* **2020**, *20*, 5359.
[25] M. Ramos, F. Marques-Moros, D. L. Esteras, S. Mañas-Valero, E. Henríquez-Guerra, M. Gadea, J. J. Baldoví, J. Canet-Ferrer, E. Coronado, M. R Calvo, *ACS Appl. Mater. Interfaces.* **2022**, *14*, 33482.
[26] C. Qin, Y. Geng, Z. Zhou, J. Song, S. Ma, G. Jia, Z. Jiao, Z. Zhu, Y. Jiang, *Opt. Express.* **2023**, *31*, 2593.
[27] Z. Chen, S. Berciaud, C. Nuckolls, T. F. Heinz, L. E. Brus, *ACS Nano.* **2010**, *4*, 2964.
[28] S. H. Amsterdam, T. K. Stanev, L. Wang, Q. Zhou, S. Irgen-Gioro, S. Padgaonkar, A. A. Murthy, V. K. Sangwan, V. P. Dravid, E. A. Weiss, P. Darancet, M. K. Y. Chan, M. C. Hersam, N. P. Stern, T. J. Marks, *J. Am. Chem. Soc.* **2021**, *143*, 17153.
[29] A. O. A. Tanoh, N. Gauriot, G. Delport, J. Xiao, R. Pandya, J. Sung, J. Allardice, Z. Li, C. A. Williams, A. Baldwin, S. D. Stranks, A. Rao, *ACS Nano.* **2020**, *14*, 15374.
[30] D. Prasai, A. R. Klots, A. Newaz, J. S Niezgoda, N. J. Orfield, C. A. Escobar, A. Wynn, A. Efimov, G. K Jennings, S. J. Rosenthal, K. I. Bolotin, *Nano Lett.* **2015**, *15*, 4374.
[31] A. Asaithambi, N. Kazemi Tofighi, M. Ghini, N. Curreli, P. J Schuck, I. Kriegel, *Chem. Commun.* **2023**, *59*, 7717.
[32] S. Sampat, T. Guo, K. Zhang, J. A. Robinson, Y. Ghosh, K. P. Acharya, H. Htoon, J. A. Hollingsworth, Y. N. Gartstein, A. V. Malko, *ACS Photonics.* **2016**, *3*, 708.
[33] N. Mutz, S. Park, T. Schultz, S. Sadofev, S. Dalgleish, L. Reissig, N. Koch, E. J. W. List-Kratochvil, S. Blumstengel, *J. Phys. Chem. C.* **2020**, *124*, 2837.
[34] Y. Wang, A. Slassi, M.-A. Stoeckel, S. Bertolazzi, J. Cornil, D. Beljonne, P. Samorì, *J. Phys. Chem. Lett.* **2019**, *10*, 540.
[35] H. Zhou, C. Qin, R. Chen, W. Zhou, G. Zhang, Y. Gao, L. Xiao, S. Jia, *J. Phys. Chem. Lett.* **2019**, *10*, 2849.
[36] F. Prins, A. J. Goodman, W. A. Tisdale, *Nano Lett.* **2014**, *14*, 6087.
[37] T. Zhu, L. Yuan, Y. Zhao, M. Zhou, Y. Wan, J. Mei, L. Huang, *Sci. Adv.* **2018**, *4*, eaao3104.
[38] J. Gu, X. Liu, E.-C. Lin, Y.-H. Lee, S. R. Forrest, V. M. Menon, *ACS Photonics.* **2018**, *5*, 100.
[39] S. Padgaonkar, P. T. Brown, Y. Jeong, C. Cherqui, K. N. Avanaki, R. López-Arteaga, S. Irgen-Gioro, Y. Wu, V. K. Sangwan, G. C. Schatz, M. C. Hersam, E. A. Weiss, *J. Phys. Chem. C.* **2021**, *125*, 15458.
[40] A. Raja, A. Montoya?Castillo, J. Zultak, X.-X. Zhang, Z. Ye, C. Roquelet, D. A. Chenet, A. M. van der Zande, P. Huang, S. Jockusch, J. Hone, D. R. Reichman, L. E. Brus, T. F. Heinz, *Nano Lett.* **2016**, *16*, 2328.
[41] A. Asaithambi, N. Kazemi Tofighi, N. Curreli, M. De Franco, A. Patra, N. Petrini, D. Baranov, L. Manna, F. D. Stasio, I. Kriegel, *Adv. Opt. Mater.* **2022**, *10*, 2200638.
[42] N. Taghipour, P. L. Hernandez Martinez, A. Ozden, M. Olutas, D. Dede, K. Gungor, O. Erdem, N. K. Perkgoz, H. V. Demir, *ACS Nano.* **2018**, *12*, 8547.

[43] J. Zhou, J. Chen, Y. Ge, Y. Shao, *Nanophotonics.* **2020**, *9*, 1855.
[44] Y. Liu, H. Li, X. Zheng, X. Cheng, T. Jiang, *Opt. Mater. Express.* **2017**, *7*, 1327.
[45] X. Zhan, Z. Tan, B. Domercq, Z. An, X. Zhang, S. Barlow, Y. Li, D. Zhu, B. Kippelen, S. R. Marder, *J. Am. Chem. Soc.* **2007**, *129*, 7246.
[46] W. Yan, Z. He, J. Jiang, D. Lu, Y. Gong, W. Yang, R. Xia, W. Huang, H. Xin, *J. Mater. Chem. C.* **2020**, *8*, 14773.
[47] C. B. Nielsen, S. Holliday, H.-Y. Chen, S. J. Cryer, I. McCulloch, *Acc. Chem. Res.* **2015**, *48*, 2803.
[48] H. Sun, X. Song, J. Xie, P. Sun, P. Gu, C. Liu, F. Chen, Q. Zhang, Z.-K. Chen, W. Huang, *ACS Appl. Mater. Interfaces.* **2017**, *9*, 29924.
[49] D. Sun, D. Meng, Y. Cai, B. Fan, Y. Li, W. Jiang, L. Huo, Y. Sun, Z. Wang, *J. Am. Chem. Soc.* **2015**, *137*, 11156.
[50] J. A. Quintana, J. M. Villalvilla, M. Morales-Vidal, P. G. Boj, X. Zhu, N. Ruangsupapichat, H. Tsuji, E. Nakamura, M. A. Díaz-García, *Adv. Opt. Mater.* **2017**, *5*, 1700238.
[51] C. Haines, M. Chen, K. P. Ghiggino, *Sol. Energy Mater. Sol. Cells.* **2012**, *105*, 287.
[52] D. Sriramulu, S. Valiyaveettil, *Dyes Pigm.* **2016**, *134*, 306.
[53] E. Kozma, W. Mróz, F. Villafiorita-Monteleone, F. Galeotti, A. Andicsová-Eckstein, M. Catellani, C. Botta, *RSC Adv.* **2016**, *6*, 61175.
[54] M. G. Ramírez, M. Morales-Vidal, V. Navarro-Fuster, P. G. Boj, J. A. Quintana, J. M. Villalvilla, A. Retolaza, S. Merino, M. A. Díaz-García, *J. Mater. Chem. C.* **2013**, *1*, 1182.
[55] R. Muñoz-Mármol, N. Zink-Lorre, J. M. Villalvilla, P. G. Boj, J. A. Quintana, C. Vázquez, A. Anderson, M. J. Gordon, A. Sastre-Santos, F. Fernández-Lázaro, M. A. Díaz-García, *J. Phys. Chem. C.* **2018**, *122*, 24896.
[56] T. Völzer, A. Schubert, E. von der Oelsnitz, J. Schröer, I. Barke, R. Schwartz, K. Watanabe, T. Taniguchi, S. Speller, T. Korn, S. Lochbrunner, *Nanoscale Adv.* **2023**, *5*, 3348.
[57] I. K. Sideri, Y. Jang, J. Garcés-Garcés, Á. Sastre-Santos, R. Canton-Vitoria, R. Kitaura, F. Fernández-Lázaro, F. D'Souza, N. Tagmatarchis, *Angew Chem Int Ed.* **2021**, *60*, 9120.
[58] S. M. Obaidulla, M. R. Habib, Y. Khan, Y. Kong, T. Liang, M. Xu, *Adv Materials Inter.* **2020**, *7*, 1901197.
[59] R. Muñoz-Mármol, P. G. Boj, J. M. Villalvilla, J. A. Quintana, N. Zink-Lorre, Á. Sastre-Santos, J. Aragó, E. Ortí, P. Baronas, D. Litvinas, S. Jursenas, F. Fenández-Lázaro, M. A. Díaz-García, *J. Phys. Chem. C.* **2021**, *125*, 12277.
[60] R. Frisenda, Y. Niu, P. Gant, A. J. Molina-Mendoza, R. Schmidt, R. Bratschitsch, J. Liu, L. Fu, D. Dumcenco, A. Kis, D. P. De Lara, A. Castellanos-Gomez, *J. Phys. D: Appl. Phys.* **2017**, *50*, 074002.
[61] S. Tongay, J. Suh, C. Ataca, W. Fan, A. Luce, J. S. Kang, J. Liu, C. Ko, R. Raghunathanan, J. Zhou, F. Ogletree, J. Li, J. C. Grossman, J. Wu, *Sci. Rep.* **2013**, *3*, 2657.
[62] R. Gómez, D. Veldman, R. Blanco, C. Seoane, J. L. Segura, R. A. J. Janssen, *Macromolecules.* **2007**, *40*, 2760.
[63] M. Katzer, S. Kovalchuk, K. Greben, K. I. Bolotin, M. Selig, A. Knorr, *Phys. Rev. B.* **2023**, *107*, 035304.
[64] P. L. Hernández-Martínez, A. O. Govorov, H. V. Demir, *J. Phys. Chem. C.* **2013**, *117*, 10203.
[65] A. A. Lutich, G. Jiang, A. S. Susha, A. L. Rogach, F. D. Stefani, J. Feldmann, *Nano Lett.* **2009**, *9*, 2636.
[66] A. K. Sheridan, A. R. Buckley, A. M. Fox, A. Bacher, D. D. C. Bradley, I. D. W. Samuel, *J. Appl. Phys.* **2002**, *92*, 6367.
[67] V. Bonal, J. A. Quintana, J. M. Villalvilla, R. Muñoz-Mármol, J. C. Mira-Martínez, P. G. Boj, M. E. Cruz, Y. Castro, M. A. Díaz-García, *Polymers.* **2021**, *13*, 2545.
[68] M. Koperski, M. R. Molas, A. Arora, K. Nogajewski, A. O. Slobodeniuk, C. Faugeras, M. Potemski, *Nanophotonics.* **2017**, *6*, 1289.
[69] R. Frisenda, E. Navarro-Moratalla, P. Gant, D. Pérez De Lara, P. Jarillo-Herrero, R. V. Gorbachev, A. Castellanos-Gomez, *Chem. Soc. Rev.* **2018**, *47*, 53.